

## Electronic Supplementary Information

### **Metal-Organic Frameworks-Derived Indium-Copper Bimetallic Oxide Catalysts for Selective Aqueous Electroreduction of CO<sub>2</sub>**

*Weiwei Guo,<sup>a,b</sup> Xiaofu Sun,<sup>\*a,b</sup> Chunjun Chen,<sup>a,b</sup> Dexin Yang,<sup>a,b</sup> Lu Lu,<sup>a,b</sup> Youdi Yang<sup>a,b</sup> and  
Buxing Han<sup>\*a,b</sup>*

*<sup>a</sup> Beijing National Laboratory for Molecular Sciences, CAS Key Laboratory of Colloid and Interface and Thermodynamics, CAS Research/Education Center for Excellence in Molecular Sciences, Institute of Chemistry, Chinese Academy of Sciences, Beijing 100190, People's Republic of China.*

*E-mail: [sunxiaofu@iccas.ac.cn](mailto:sunxiaofu@iccas.ac.cn); [hanbx@iccas.ac.cn](mailto:hanbx@iccas.ac.cn)*

*<sup>b</sup> School of Chemistry and Chemical Engineering, University of Chinese Academy of Sciences, Beijing 100049, People's Republic of China.*

## Contents

Experimental Section-----	3
Supplementary Figures-----	6
Supplementary Tables-----	18
References -----	22

## Experimental Section

### Materials

N,N-Dimethylformamide was obtained from J&K Scientific Ltd.  $\text{In}(\text{NO}_3)_3 \cdot 6\text{H}_2\text{O}$ ,  $\text{Cu}(\text{NO}_3)_2 \cdot 3\text{H}_2\text{O}$ , Terephthalic acid (98+%), Toray Carbon Paper (CP, TGP-H-60, 19×19 cm) and Nafion N-117 membrane (0.180 mm thick,  $\geq 0.90$  meg/g exchange capacity) were purchased from Alfa Aesar China Co., Ltd.  $\text{CO}_2$  (99.999 %) and  $\text{N}_2$  (99.99 %) were provided by Beijing Analytical Instrument Company.

### Catalysts preparation

For the synthesis of the InCu-MOF (Cu/In = 1), 1 mmol of terephthalic acid was dissolved in 20 mL of DMF. Then, 1 mmol of  $\text{In}(\text{NO}_3)_3 \cdot 6\text{H}_2\text{O}$  and 1 mmol of  $\text{Cu}(\text{NO}_3)_2 \cdot 3\text{H}_2\text{O}$  were added and stirred at room temperature for 2 h. Subsequently, the solution was heated at 120 °C in an oil bath for 1 h. The precipitate was obtained after cooling to room temperature. The precipitate was centrifuged, followed by washing with DMF and deionized water and then dried at 80 °C overnight in a vacuum oven. After that, the mixture was placed in a crucible and heated at 400 °C in the muffle for 4 h. The product was obtained after cooling to room temperature and then electrochemically reduced at -1.4 V vs. RHE for 20 min. The final product can be obtained.

### Catalysts characterization

The actual compositions of In and Cu in the InCuO-x catalysts were determined by inductively coupled plasma optical emission spectroscopy (ICP-OES, Vista-MPX). X-ray photoelectron spectroscopy (XPS) analysis was performed on the Thermo Scientific ESCA Lab 250Xi using 200 W monochromatic Al K $\alpha$  radiation. The 500  $\mu\text{m}$  X-ray spot was used. The base pressure in the analysis chamber was about  $3 \times 10^{-10}$  mbar. Typically, the hydrocarbon C1s line at 284.8 eV from adventitious carbon was used for energy referencing X-ray diffraction (XRD) analysis of the samples was performed on the X-ray diffractometer (Model D/MAX2500, Rigaku) with Cu-K $\alpha$  radiation, and the scan speed was 5° min<sup>-1</sup>. The morphologies of as-synthesized materials were characterized by a HITACHI S-4800 scanning electron microscope (SEM) and a JEOL JEM-2100F high-resolution transmission electron microscopy (HR-TEM).  $\text{N}_2$  adsorption/desorption isotherms of the materials were determined using a Quadrasorb SI-MP system to obtain Brunauer-Emmett-Teller (BET) specific surface area and pore size. The adsorption isotherms of  $\text{CO}_2$  were determined at 25 °C in the pressure range of 0-1 atm on a TriStar II 3020 device.

### Electrode preparation

To prepare the InCuO-x/CP electrode, 10 mg catalyst was suspended in 1 mL acetone with 20  $\mu\text{L}$  Nafion D-521 dispersion (5 wt%) to form a homogeneous ink. Then, 500  $\mu\text{L}$  of solution was spread onto the CP (1×1 cm<sup>2</sup>) surface by a micropipette and then dried under room temperature. The loading of catalyst was 5.0 mg cm<sup>-2</sup>. Before experiment, all the auxiliary electrodes were sonicated in acetone for 10 min and then washed with water and ethanol, followed by drying in  $\text{N}_2$  atmosphere.

### Electrocatalytic $\text{CO}_2$ reduction

All the electrochemical experiments were conducted on the electrochemical workstation (CHI

6081E). All potentials cited in this work were referenced to the RHE, unless stated otherwise. The reference potentials were converted to RHE using the formulas  $E(\text{vs RHE}) = E(\text{vs Ag/AgCl}) + 0.197 \text{ V} + 0.0591 \times \text{pH}$ .<sup>S1</sup> The electrolysis experiments were conducted at 25 °C in a H-type cell with a working cathode, a counter anode (platinum gauze), and a reference electrode (Ag/AgCl with saturated KCl).<sup>S2, S3</sup> In the experiment, Nafion-117 membrane was used as the proton exchange membrane that separated the cathode and anode compartments. KHCO<sub>3</sub> aqueous solution (0.5 M) was utilized as electrolyte. In each experiment, the amount of electrolyte was 30 mL. Before starting the electrolysis experiment, the catholyte was bubbled with CO<sub>2</sub> for 30 min under stirring and the electrolysis was carried out under a steady stream of CO<sub>2</sub> (2 sccm).

### **Product analysis**

The gaseous product of electrochemical experiments was collected using a gas bag and analyzed by gas chromatography (GC, HP 4890D), which was equipped with FID and TCD detectors using helium as the internal standard. The liquid product was analyzed by <sup>1</sup>H NMR (Bruker Avance III 400 HD spectrometer) in DMSO-d<sub>6</sub> with TMS as an internal standard.

### **Gaseous products**

FE = moles of products per second / theoretical moles equivalent per second

From the GC peak areas and calibration curves for the TCD detector, the V % of CO (or H<sub>2</sub>) could be obtained. Since the flow rate of the gas was controlled, the amount of moles of CO (or H<sub>2</sub>) per second could be calculated. The theoretical moles per second were obtained from current density since production of CO (or H<sub>2</sub>) proceeded via 2-electron paths.

### **Tafel analysis**

The partial current densities for products under different potentials were measured. The overpotential was obtained from the difference between the equilibrium potential and the catalytic potential. Multiple electrolysis experiments were performed at each potential to obtain the current density versus overpotential data in the H-type electrolysis cell as described above. Tafel plots were constructed from these data.

### **Normalized current density and electrochemical surface areas (ECSAs) study**

The cyclic voltammetry measurement was conducted in 0.5 M KHCO<sub>3</sub> solution using a three-electrode system at 25 °C. Cyclic voltammogram measurements of the six catalysts were conducted from -0.35 to -0.45 V vs RHE with various scan rates to obtain the double layer capacitance (C<sub>dl</sub>) of indium-copper bimetallic oxides. The C<sub>dl</sub> was estimated by plotting the  $\Delta j$  ( $j_a - j_c$ ) at -0.4 V vs RHE against the square root of scan rates, in which  $j_a$  and  $j_c$  were the anodic and cathodic current density, respectively. The linear slope was equivalent to twice of the C<sub>dl</sub>. The electrochemical surface areas (ECSAs) was calculated by the following equation:  $\text{ECSAs} = R_f S$ , where  $R_f$  represented the roughness factor of catalyst surface and  $S$  represented the surface area of the carbon paper electrode. Based on the C<sub>dl</sub> of a smooth oxide surface,  $R_f$  can be calculated according to the relation  $R_f = C_{dl}/a$  in this case. The surface roughness factor of In<sub>2</sub>O<sub>3</sub> was defined to be 1, and the normalized current density of CO can be calculated according to the surface roughness factor of the different catalysts.

### **Electrochemical impedance spectroscopy (EIS) study**

The experimental apparatus was the same as that for LSV measurements. The EIS measurement was carried out in 0.5 M  $\text{KHCO}_3$  at an open circuit potential (OCP). The data obtained from the EIS measurements were fitted by the software of Zview (Version 3.1, Scribner Associates, USA). The electrical equivalent circuit used for simulating the experimental impedance data has been given in Fig. S14.

## Supplementary Figures

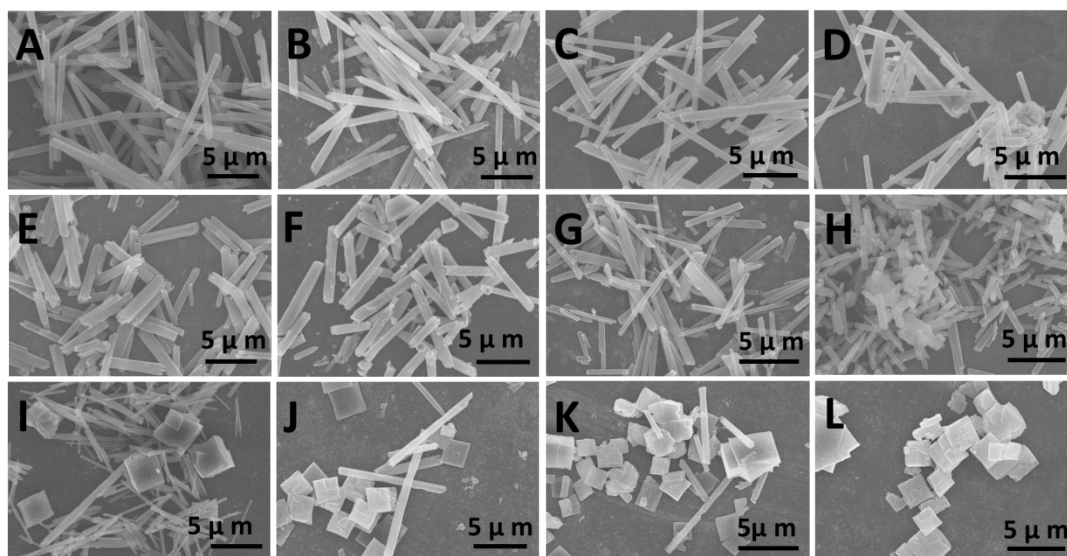


**Fig. S1** SEM images of In-Cu bimetallic MOFs with the different Cu/In ratios (A: 0/5; B: 1/5; C: 2/5; D: 3/5; E: 4/5; F: 5/5; G: 6/5; H: 3/2; I: 2/1; J: 3/1; K: 4/1 and L: 5/0).

There are two reasons for selecting In-Cu MOFs in this work. On the one hand, the MOFs are made of In/Cu and terephthalic acid. The porous bimetallic oxides can be easily designed by handy and efficient way for thermal decomposition of MOFs under air atmosphere. The desired In-Cu ratio was designable and easily controlled by changing the precursor ratios. On the other hand, we want to synthesize metal oxides without introducing other heteroatoms. Terephthalic acid is an excellent ligand for this. Therefore, In-Cu MOFs were chosen as the precursors for preparing In-Cu bimetallic oxides.

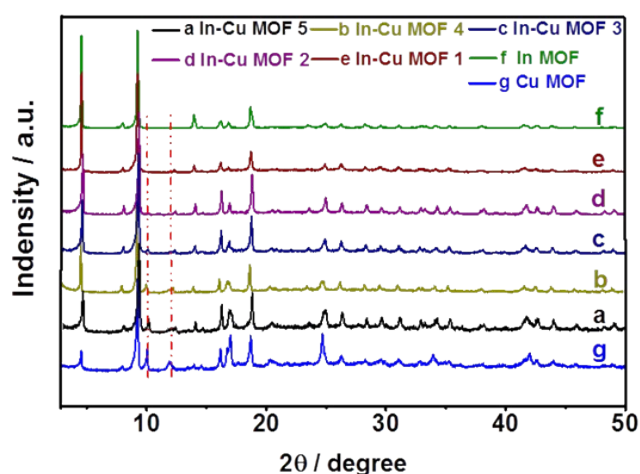


**Fig. S2** XRD patterns of In-Cu bimetallic MOFs with different Cu/In ratios.

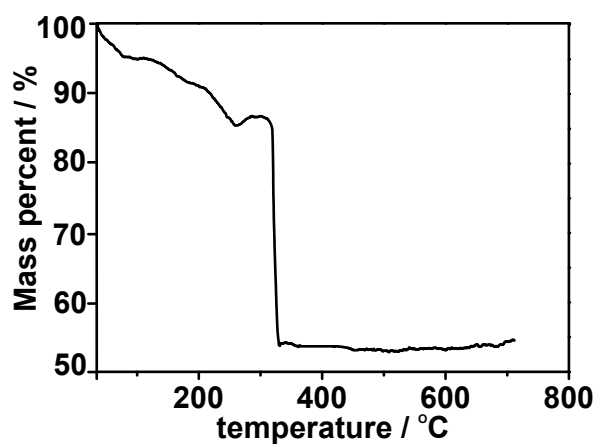


**Fig. S3** TG of the In-Cu bimetallic MOF.

As shown in Fig. S3, the initial weight loss at the temperature range of 30-120°C corresponds to the physical desorption of surface adsorbing water and ethanol (approximately 5%). And then, a flat weight loss (approximately 10%) from 120 °C to 310 °C may be corresponds to decompose of DMF coordinated in the hole. Finally, a sharp weight loss from 310 °C to 320 °C may be due to decomposition of organic BDC linker (approximately 30%) and the crystal structure collapsed to CuO, In<sub>2</sub>O<sub>3</sub> and volatile compounds. The actual volatile compound was CO<sub>2</sub>, which were determined by in-situ MS.

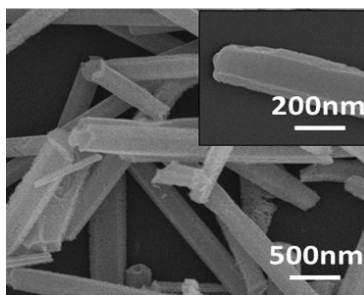


**Fig. S4** SEM images of In<sub>2</sub>O<sub>3</sub>.

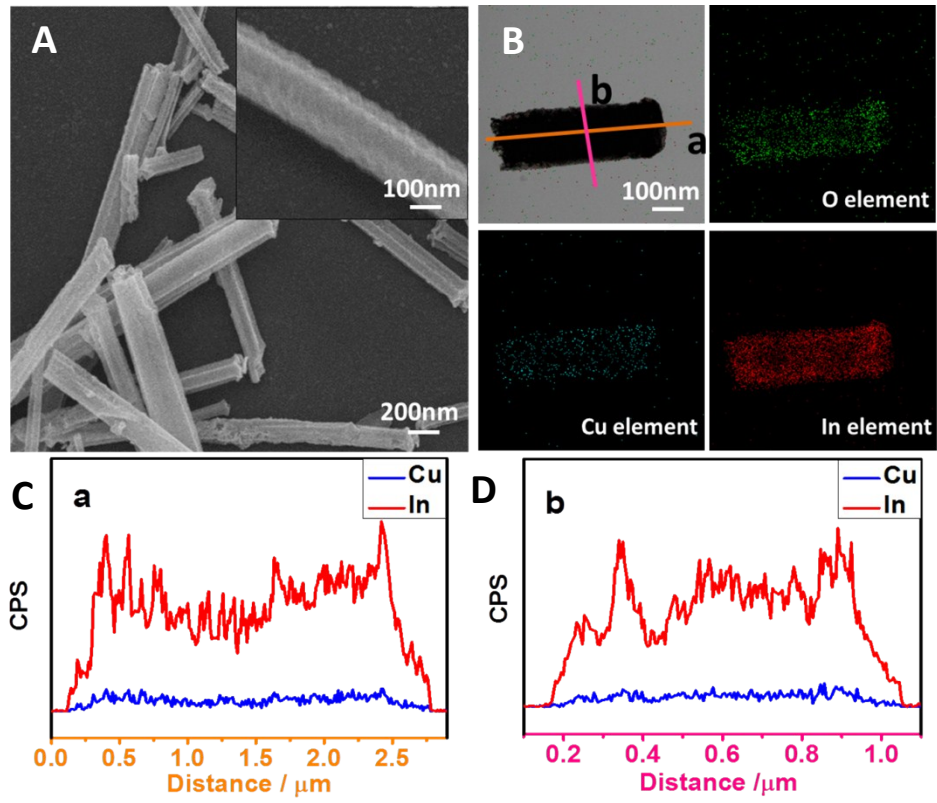


**Fig. S5A)** SEM images B) elemental mappings C, D) line scanning images of **InCuO-0.15**.

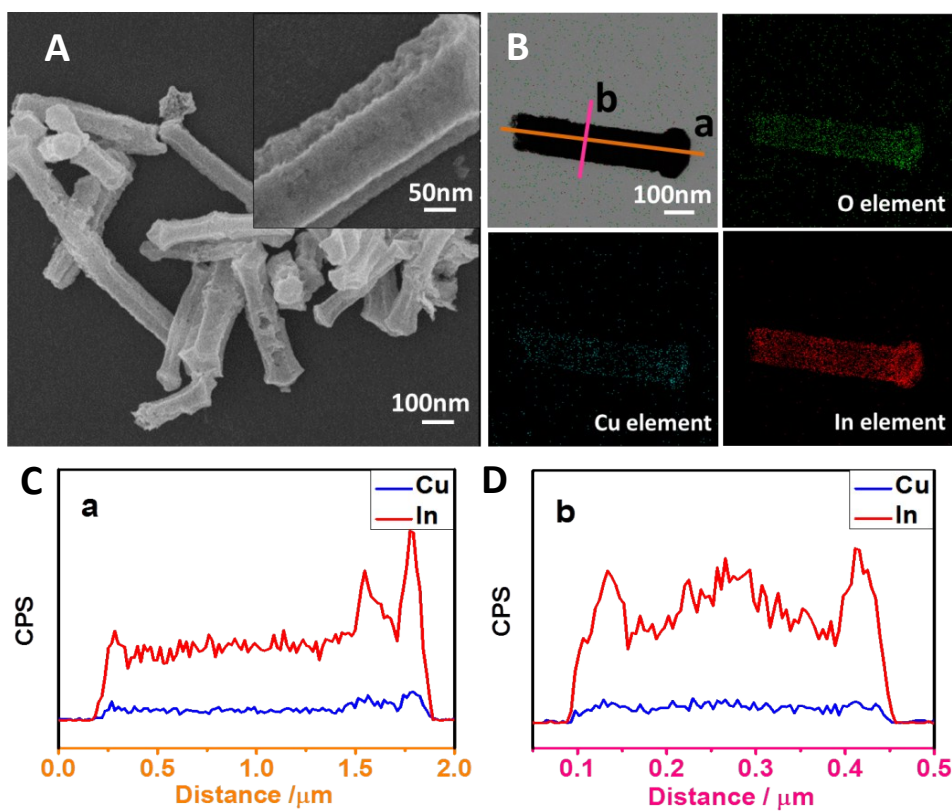


**Fig. S6** A) SEM images B) elemental mappings C,D) line scanning images of **InCuO-0.37**.

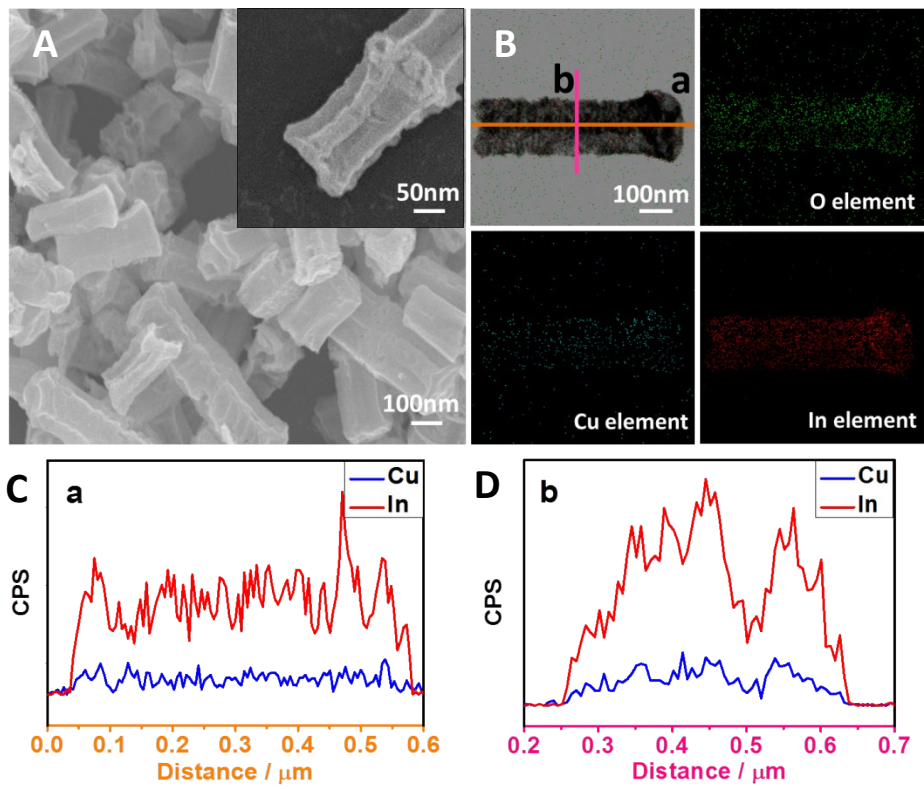


**Fig. S7** A) SEM images B) elemental mappings C,D) line scanning images of  $\text{InCuO-0.55}$ .

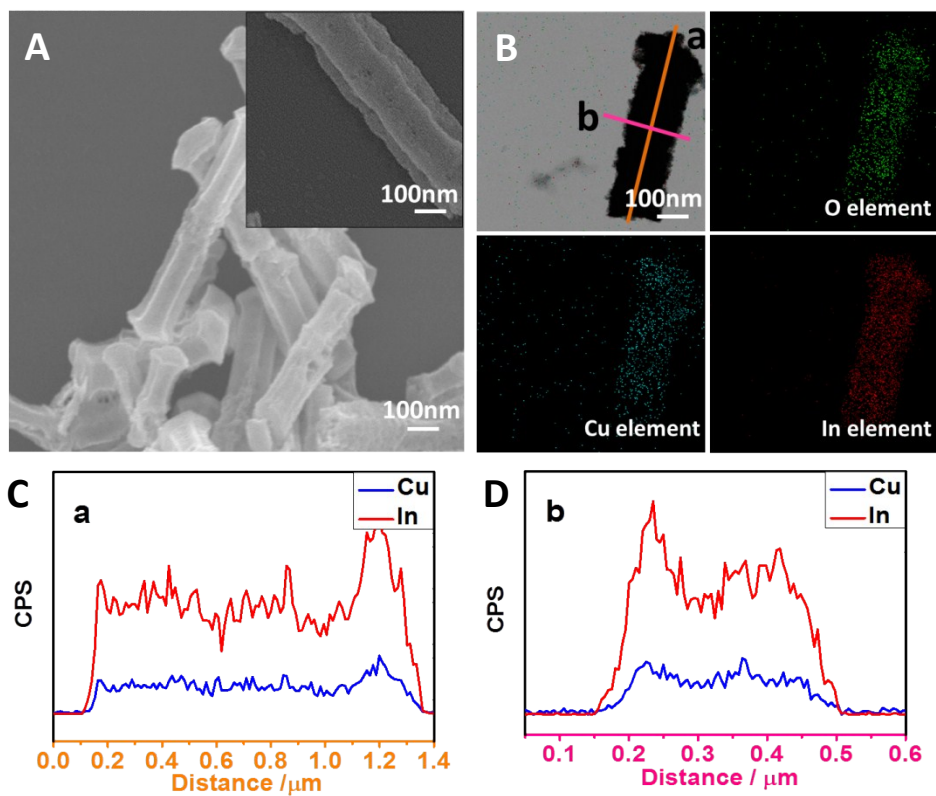


**Fig. S8** A) SEM images B) elemental mappings C,D) line scanning images of  $\text{InCuO}_{0.72}$ .

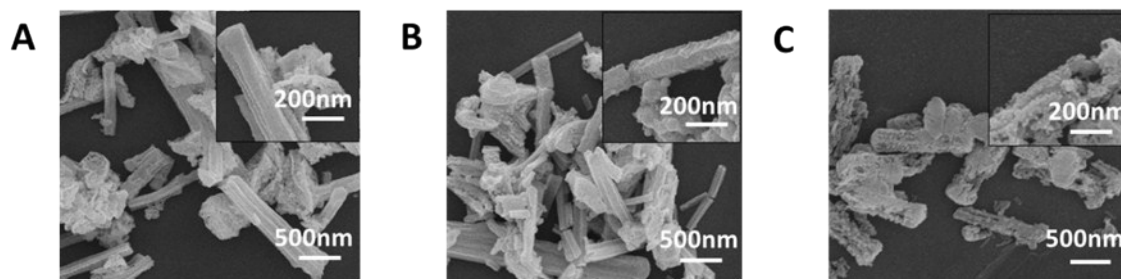


Fig. S9 SEM images of A) InCuO-1.52, B) InCuO-1.96, and C) InCuO-2.98.

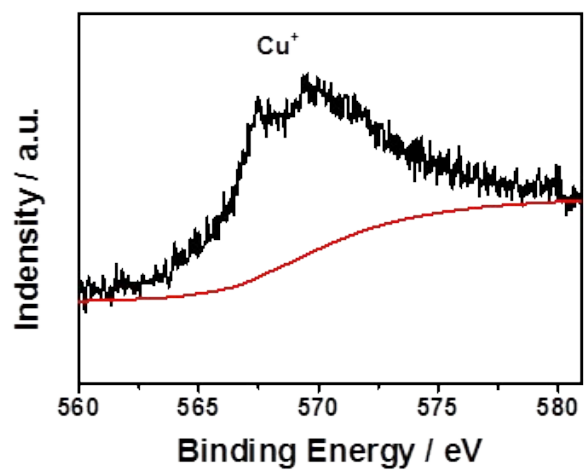
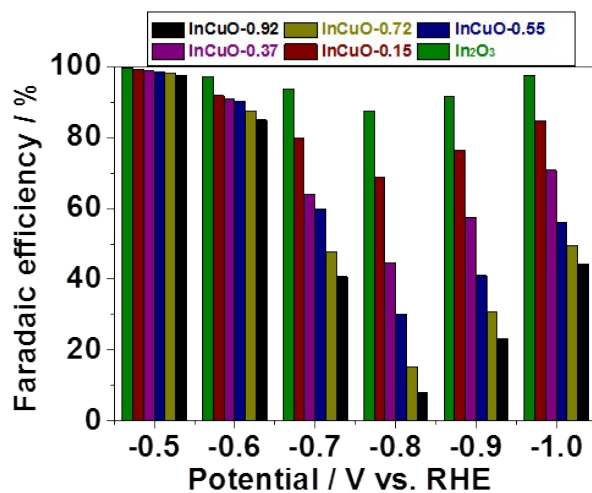
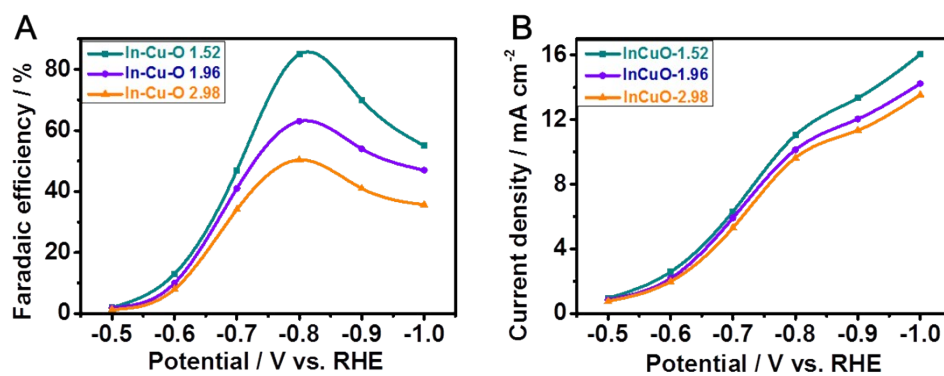


Fig. S10 AES spectrum of Cu LMM of InCuO-0.92.



**Fig. S11** Faradaic efficiency of H<sub>2</sub> for different catalysts at the applied potentials.



**Fig. S12** Faradaic efficiency for CO and the total current density over InCuO-1.52, InCuO-1.96 and InCuO-2.98 at the applied potentials.

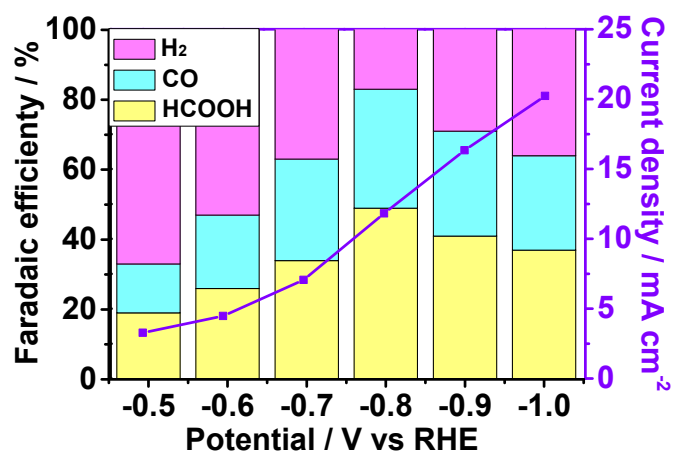


Fig. S13 Faradaic efficiency and the total current density over Cu oxide at the applied potentials.

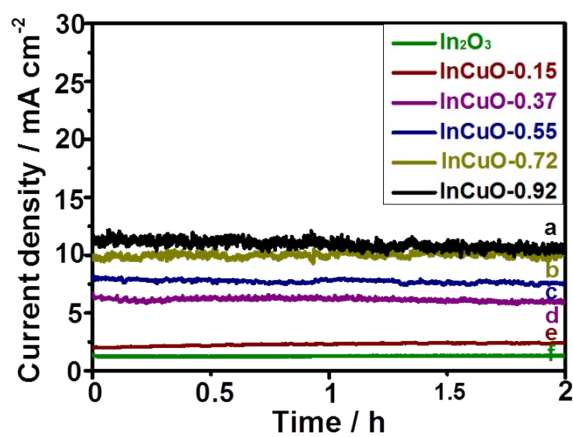
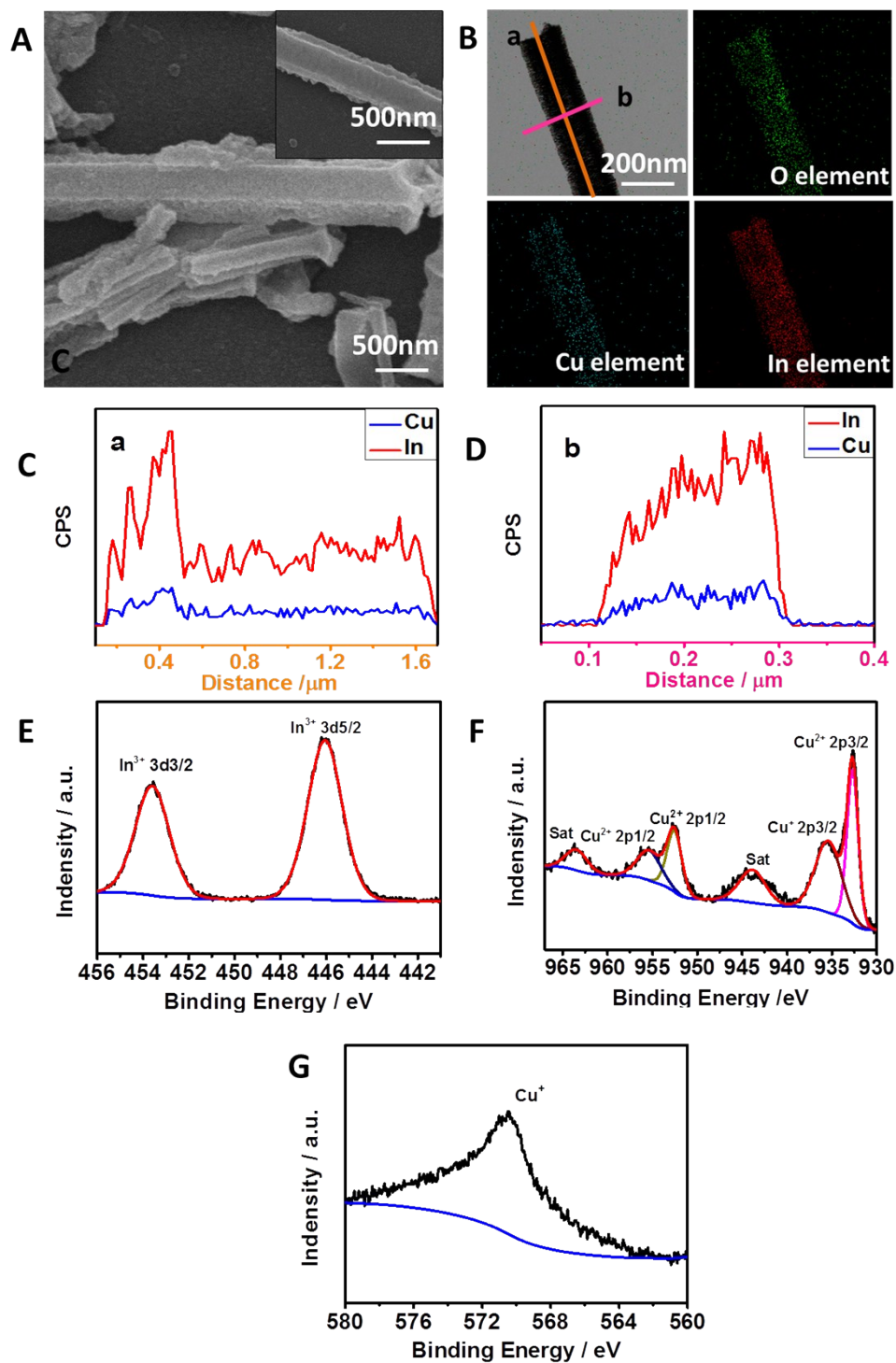
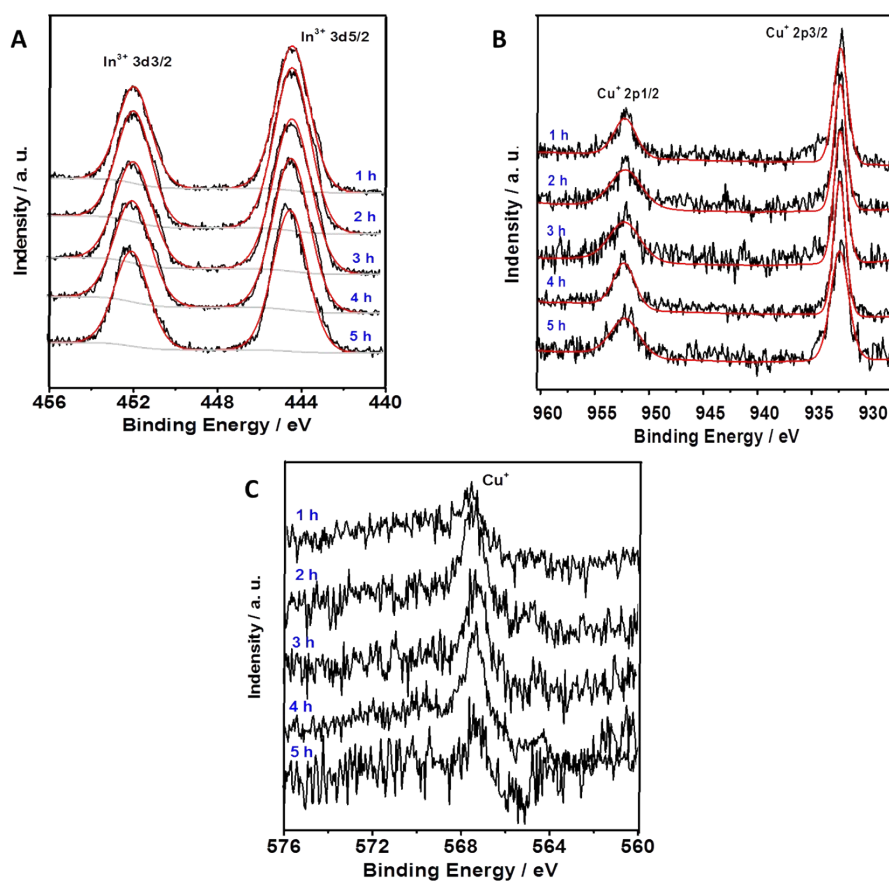


Fig. S14 The stability of different catalysts at -0.8 V vs. RHE during 2 h electrolysis.



**Fig. S15** A) SEM image of  $\text{InCuO-0.92}$  after electrolysis for 2 h. B) Elemental mappings and C,D) line scanning image of  $\text{InCuO-0.92}$  after electrolysis. XPS spectra of the catalyst: high resolution spectra of In 3d E) and Cu 2p F) of  $\text{InCuO-0.92}$  after electrolysis. G) AES spectrum of Cu LMM after electrolysis.



**Fig. S16** Semi-XPS spectra of the catalyst: high resolution spectra of In 3d A) and Cu 2p B) of **InCuO-0.92** in electrolysis. C) Semi-AES spectrum of Cu LMM in electrolysis.

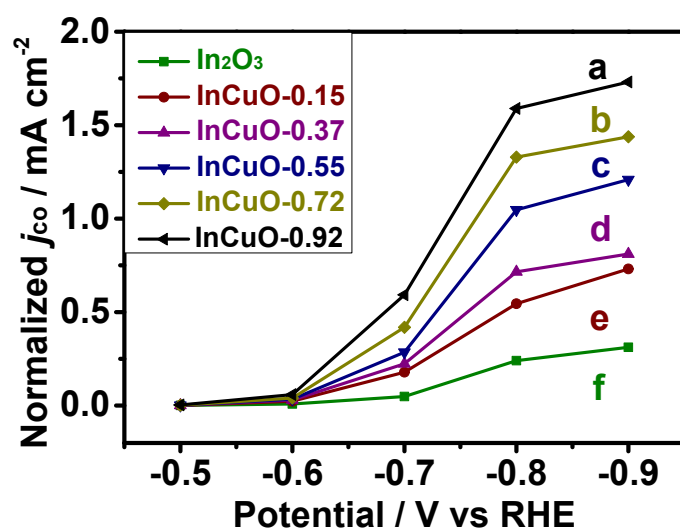


Fig. S17 ECSA-normalized current density for CO at selected potentials.

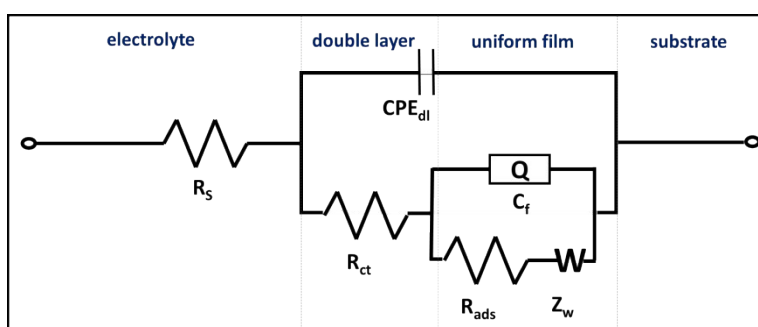


Fig. S18 Electrical equivalent circuit used for simulating the experimental impedance data.

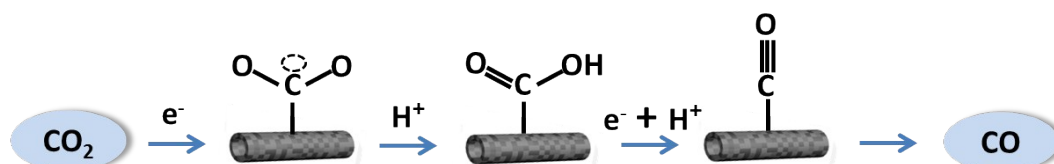


Fig. S19 Schematic demonstration of a possible mechanism for the electrocatalytic reduction of aqueous CO<sub>2</sub> to CO.

## Supplementary Tables

**Table S1.** Summary of representative MOF-based materials for the electrochemical reduction of CO<sub>2</sub>

Electrode	Electrolyte	Product, FE / %	Current density / mA cm <sup>-2</sup>	Ref.
AL <sub>2</sub> (OH) <sub>2</sub> TCPP-Co	0.5 M KHCO <sub>3</sub>	CO 76%	5.9	[S4]
Fe_MOF-525	1 M TBAPF <sub>6</sub> acetonitrile solution	CO ~54%	2.3	[S5]
Cu <sub>3</sub> (BTC) <sub>2</sub>	DMF/TBATFB solution	oxalic acid 51%	-	[S6]
Cu <sub>2</sub> O/ZnO	2-methylpyridine - based system with a pH of 7.6	methanol 12%	1	[S7]
CuAdeAce	0.1 M KHCO <sub>3</sub>	methanol and ethanol	10	[S8]
CR-MOFs	0.5 M KHCO <sub>3</sub>	HCOOH 98%	-	[S9]
Cu-MOF-5	-	HCOOH	-	[S10]
RE- SURMOF	0.1 M TBAH with 5% triuoroethanol	CO ~93%	2	[S11]
Zn-MOF/CP	BmimBF <sub>4</sub>	CH <sub>4</sub> 80.1 ± 6.6%	3.1	[S2]
surface functionalized ZIF-8	1 M KHCO <sub>3</sub>	CO 89.1%	~5	[S12]
CuPc	0.5 M KHCO <sub>3</sub>	Methane 66%	13	[S13]
ZIF-CNT-FA-p	0.1 M NaHCO <sub>3</sub>	CO 100%	7.7	[S14]

**Table S2** The ICP results of different catalysts.

Material	In / wt%	Cu / wt%	Cu / In atomic ratio
<b>InCuO-0.15</b>	59.0	5.0	0.15
<b>InCuO-0.37</b>	49.4	10.2	0.37
<b>InCuO-0.55</b>	46.2	14.0	0.55
<b>InCuO-0.72</b>	43.0	17.1	0.72
<b>InCuO-0.92</b>	39.7	20.2	0.92
<b>InCuO-1.52</b>	32.5	27.4	1.52
<b>InCuO-1.96</b>	28.3	30.9	1.96
<b>InCuO-2.98</b>	22.6	37.4	2.98

**Table S3** The BET surface area and adsorption average pore size of different catalysts.

Material	BET Surface Area / m <sup>2</sup> g <sup>-1</sup>	Adsorption Average Pore Size / nm
<b>In<sub>2</sub>O<sub>3</sub></b>	91.9	12.7
<b>InCuO-0.15</b>	104.1	11.8
<b>InCuO-0.37</b>	116.8	9.5
<b>InCuO-0.55</b>	146.2	7.6
<b>InCuO-0.72</b>	162.8	4.0
<b>InCuO-0.92</b>	218.4	3.9

Electrode	Electrolyte	Product, FE / %	Current density / mA cm <sup>-2</sup>	Ref.
<b>InCuO-0.92</b>	0.5 M KHCO <sub>3</sub>	CO 92.1%	11.2	This work
Cu-In alloy	0.1 M KHCO <sub>3</sub>	CO 95%	1.67	[S15]
One-dimensional CuIn alloy nanowires	0.5 M KHCO <sub>3</sub>	CO 68.2%	2.66	[S16]
Cu/In Interface	0.1 M KHCO <sub>3</sub>	CO 93%	4	[S17]
Cu-In nanoalloys	0.1 M KHCO <sub>3</sub>	CO 56%	1.5	[S18]
Cu-In alloy	0.1 M KHCO <sub>3</sub>	CO 63%	1.67	[S19]
Cu-In alloy	0.1 M KHCO <sub>3</sub>	CO ~ 4 % Formate 62 %	1.5	[S20]
Cu-In alloy	0.5 M KHCO <sub>3</sub>	CO ~90%	3	[S21]
Immobilized Indium(III) Protoporphyrin	0.1 M phosphate buffer with pH 9.6	HCOOH ~75%	~28	[S22]
Nanofibrous CuInS <sub>2</sub>	0.1 M TBAPF <sub>6</sub> in acetonitrile.	CO 77 ± 4%	0.22	[S23]

**Table S4.** Comparison of CO<sub>2</sub> reduction performance on different Cu-In catalysts.

Generally, Cu-In was a promising catalyst for CO<sub>2</sub>RR. Kazuhiro Takanabe et al reported a Cu-In alloy. The Cu-In electrode selectively converted CO<sub>2</sub> to CO with a Faradaic efficiency of about 95% and the current density of 1.67 mA cm<sup>-2</sup>.<sup>S15</sup> Andreas Züttel et al designed Cu nanowire-supported In catalysts as advanced electrocatalysts for the aqueous electroreduction of CO<sub>2</sub>, the catalyst exhibited a CO Faradaic efficiency of ~93% at -0.6 to -0.8 V vs RHE.<sup>S17</sup> Javier Perez-Ramírez et al<sup>S18</sup> prepared Cu-In nanoalloys for CO evolution. Kazuhiro Takanabe<sup>S19</sup> et al reported the generation of Cu-In alloy surfaces for electrochemical reduction of CO<sub>2</sub>. The material

successfully generated selective active sites to form CO from CO<sub>2</sub> electroreduction and the FEs of H<sub>2</sub> (6%), CO (63%), and HCOOH (31%) at  $\sim -0.7$  V vs. RHE (Table S4). In this work, very high current density and mass activity for CO production was achieved by using MOF-derived In-Cu bimetallic oxide catalysts, which can be attributed to the synergistic effect Cu and In for electrocatalytic CO<sub>2</sub> reduction.

Electrode	Electrolyte	Product, FE / %	Current density / mA cm <sup>-2</sup>	Ref.
OD Cu/C (HKUST-1)	0.1 M KHCO <sub>3</sub>	alcohol compounds	1.0	[S24]
Ni SAs/N-C derived ZIF-8	0.5 M KHCO <sub>3</sub>	CO 71.9%	10.48	[S25]
Fe-N-C	0.5 M NaHCO <sub>3</sub>	CO 91%	7.5	[S26]
Co-N <sub>2</sub>	0.5 M KHCO <sub>3</sub>	CO 94%	18.1	[S27]
Ag/Co <sub>3</sub> O <sub>4</sub>	0.1 M KHCO <sub>3</sub>	CO 55.6%	$\sim 20$	[S28]
Cu <sub>3</sub> NiOCs	0.5 M KHCO <sub>3</sub>	HCOOH 95.9%	10.9	[S29]
Ni-NC_X@C	0.5 M KHCO <sub>3</sub>	CO 94%	22.7	[S30]
FeMn-N-C	0.1 M KHCO <sub>3</sub>	CO 80%	6 mA g <sup>-1</sup>	[S31]

**Table S5.** Summary of representative MOF-derived materials for the electrochemical reduction of CO

## References

- S1 J. Shen, R. Kortlever, R. Kas, Y. Y. Birdja, O. Diaz-Morales, Y. Kwon, I. Ledezma-Yanez, K. J. P. Schouten, G. Mul, M. T. Koper, *Nat. Commun.*, 2015, **6**, 9177.
- S2 X. Kang, Q. Zhu, X. Sun, J. Hu, J. Zhang, Z. Liu, B. Han, *Chem. Sci.*, 2016, **7**, 266-273.
- S3 X. Sun, X. Kang, Q. Zhu, J. Ma, G. Yang, Z. Liu, B. Han, *Chem. Sci.*, 2016, **7**, 2883-2887.
- S4 N. Kornienko, Y. Zhao, C. S. Kley, C. Zhu, D. Kim, S. Lin, C. J. Chang, O. M. Yaghi and P. Yang, *J. Am. Chem. Soc.*, 2015, **137**, 14129-14135.
- S5 I. Hod, M. D. Sampson, P. Deria, C. P. Kubiak, O. K. Farha and J. T. Hupp, *ACS Catal.*, 2015, **5**, 6302-6309.
- S6 R. S. Kumara, S. S. Kumarb, M. A. Kulandainathan, *Electrochem. Commun.*, 2012, **25**, 70-73.
- S7 J. Albo, G. Beobide, P. Castaño, A. Irabien, *J. CO<sub>2</sub> Util.*, 2017, **18**, 164-172.
- S8 J. Albo, D. Vallejo, G. Beobide, O. Castillo, P. Castano, A. Irabien, *ChemSusChem*, 2017, **10**, 1100-1109.
- S9 R. Hinogami, S. Yotsuhashi, M. Deguchi, Y. Zenitani, H. Hashiba, Y. Yamada, *ECS Electrochem. Lett.*, 2012, **1**, H17-H19.
- S10 T. Maihom, S. Wannakao, B. Boekfa, J. Limtrakul, *J. Phys. Chem. C*, 2013, **117**, 17650-17658;
- S11 L. Ye, J. Liu, Y. Gao, C. Gong, M. Addicoat, T. Heine, C. Woill and L. Sun, *J. Mater. Chem. A*, 2016, **4**, 15320-15326.
- S12 Y. Ye, F. Cai, H. Li, H. Wu, G. Wang, Y. Li, S. Miao, S. Xie, R. Si, J. Wang and X. Bao, *Nano Energy*, 2017, **38**, 281-289.
- S13 Z. Weng, Y. Wu, M. Wang, J. Jiang, K. Yang, S. Huo, X.-F. Wang, Q. Ma, G. W. Brudvig, V. S. Batista, Y. Liang, Z. Feng, H. Wang, *Nat. Commun.*, 2018, **9**, 415.
- S14 Y. Guo, H. Yang, X. Zhou, K. Liu, C. Zhang, Z. Zhou, C. Wang, W. Lin, *J. Mater. Chem. A*, 2017, **5**, 24867-24873.
- S15 Rasul, D. H. Anjum, A. Jedidi, Y. Minenkov, L. Cavallo, and K. Takanabe, *Angew. Chem. Int. Ed.*, 2015, **54**, 2146-2150.
- S16 Y. J. Janga, J. Leeb, J. Kima, B. J. Leea and J. S. Leea, *J. Power Sources*, 2018, **378**, 412-417.
- S17 W. Luo, W. Xie, R. Mutschler, E. Oveisi, G. Luca De Gregorio, R. Buonsanti and An. Züttel, *ACS Catal.*, 2018, **8**, 6571-6581.
- S18 G. O. Larrazábal, A. J. Martín, S. Mitchell, R. Hauert and J. Pérez-Ramírez, *ACS Catal.*, 2016, **6**, 6265-6274.
- S19 A. Jedidi, S. Rasul, D. Masih, L. Cavallo and K. Takanabe, *J. Mater. Chem. A*, 2015, **3**, 19085-19092.

- S20 Z. B. Hoffman, T. S. Gray, K. B. Moraveck, T. B. Gunnoe and G. Zangari, *ACS Catal.*, 2017, **7**, 5381-5390.
- S21 J. He, K. E. Dettelbach, D. A. Salvatore, T. Li, C. P. Berlinguette, *Angew. Chem. Int. Ed.*, 2017, **56**, 6068-6072.
- S22 Y. Y. Birdja, R. E. Vos, T. A. Wezendonk, L. Jiang, F. Kapteijn and M. T. M. Koper, *ACS Catal.*, 2018, **8**, 4420-4428.
- S23 A. Aljabour, D. H. Apaydin, H. Coskun, F. Ozel, M. Ersoz, P. Stadler, N. S. Sariciftci and M. Kus, *ACS Appl. Mater. Interfaces*, 2016, **8**, 31695-31701.
- S24 K. Zhao, Y. Liu, X. Quan, S. Chen, H. Yu, *ACS Appl. Mater. Interfaces*, 2017, **9**, 5302-5311.
- S25 C. Zhao, X. Dai, T. Yao, W. Chen, X. Wang, J. Wang, J. Yang, S. Wei, Y. Wu and Y. Li, *J. Am. Chem. Soc.*, 2017, **139**, 8078-8081.
- S26 T. N. Huan, N. Ranjbar, G. Rousse, M. Sougrati, A. Zitolo, V. Mougel, F. Jaouen, M. Fontecave, *ACS Catal.*, 2017, **7**, 1520-1525.
- S27 X. Wang, Z. Chen, X. Zhao, T. Yao, W. Chen, R. You, C. Zhao, G. Wu, J. Wang, W. Huang, J. Yang, X. Hong, S. Wei, Y. Wu, Y. Li, *Angew. Chem. Int. Ed.*, 2018, **57**, 1944-1948.
- S28 S. Y. Zhang, Y. Y. Yang, Y. Q. Zheng and H. L. Zhu, *J. Solid State Chem.*, 2018, **263**, 44-51.
- S29 D. Yang, Q. Zhu, X. Sun, C. Chen, L. Lu, W. Guo, Z. Liu and B. Han, *Green Chem.*, 2018, **20**, 3705-3710.
- S30 M. Jia, C. Chol, T. Wu, C. Ma, P. Kang, H. Tao, Q. Fan, S. Hong, S. Liu, Y. L. Soo, Y. Jung, J. Qiu and Z. Sun, *Chem. Sci.*, 2019, DOI: 10.1039/C8SC03732A.
- S31 A. S. Varela, N. R. Sahaie, J. Steinberg, W. Ju, H.- S. Oh, P. Strasser, *Angew. Chem., Int. Ed.* 2015, **54**, 10758-10762.